High-throughput computational screening of thermal conductivity, Debye temperature, and Grüneisen parameter using a quasiharmonic Debye model

Cormac Toher,[1] Jose J. Plata,[1] Ohad Levy,[1,*] Maarten de Jong,[2] Mark Asta,[2]
Marco Buongiorno Nardelli,[3] and Stefano Curtarolo[4,†]

[1]*Department of Mechanical Engineering and Materials Science, Duke University, Durham, North Carolina 27708, USA*
[2]*Department of Materials Science and Engineering, University of California, Berkeley, 210 Hearst Memorial Mining Building, Berkeley, California 94720, USA*
[3]*Department of Physics and Department of Chemistry, University of North Texas, Denton, Texas 76203, USA*
[4]*Materials Science, Electrical Engineering, Physics, and Chemistry, Duke University, Durham, North Carolina 27708, USA*
(Received 29 July 2014; revised manuscript received 13 October 2014; published 12 November 2014)

The quasiharmonic Debye approximation has been implemented within the AFLOW and Materials Project frameworks for high-throughput computational materials science (Automatic Gibbs Library, AGL), in order to calculate thermal properties such as the Debye temperature and the thermal conductivity of materials. We demonstrate that the AGL method, which is significantly cheaper computationally compared to the fully *ab initio* approach, can reliably predict the ordinal ranking of the thermal conductivity for several different classes of semiconductor materials. In particular, a high Pearson (i.e., linear) correlation is obtained between the experimental and AGL computed values of the lattice thermal conductivity for a set of 75 compounds including materials with cubic, hexagonal, rhombohedral, and tetragonal symmetry.

DOI: 10.1103/PhysRevB.90.174107 PACS number(s): 66.70.Df

I. INTRODUCTION

Calculating the thermal properties of materials is important for predicting the thermodynamic stability of structural phases and assessing their importance for a variety of applications. The lattice thermal conductivity, κ_l, is a crucial design parameter in a wide range of important technologies, such us the development of new thermoelectric materials [1,2], heat sink materials for thermal management in electronic devices [3], and rewritable density scanning-probe phase-change memories [4]. High thermal conductivity materials, which typically have a zinc-blende or diamond-like structure, are essential in microelectronic and nanoelectronic devices to achieve efficient heat removal [5] and have been intensively studied for the past few decades [6]. Low thermal conductivity materials constitute the basis of a new generation of thermoelectric materials and thermal barrier coatings [7].

The determination of the thermal conductivity of materials is computationally demanding since it requires calculation of multiple-phonon scattering processes, which are the origin of the lattice resistance to heat transport. The methods most commonly used currently to calculate the thermal conductivity are based on solving the Boltzmann transport equation (BTE). This solution involves the calculation of the phonon frequencies, group velocities, and the harmonic and anharmonic interatomic force constants (IFCs) [8,9]. In particular, the third-order anharmonic IFCs are required in order to incorporate the effects of three phonon scattering processes [8,9]. The standard method to calculate these anharmonic IFCs is based on density functional theory (DFT). Deinzer *et al.* [10] used density functional perturbation theory (DFPT) to obtain third-order IFCs to study the phonon linewidths. In the last decade, this method has been successfully used to solve the BTE and predict the thermal conductivity of different materials [8,9,11–16]. Such evaluation of the higher-order IFCs requires electronic structure calculations for multiple large supercells, each of which has a different set of atomic displacements. These first-principles solutions of the BTE are therefore computationally extremely expensive.

A variety of simple methods have been devised to evaluate the thermal properties of materials at reduced computational cost. Early approximate implementations to compute the lattice thermal conductivity were based on semiempirical models to solve the BTE, in which some parameters are obtained from fitting to experimental data [17–19]. This reduces the predictive power of the calculations.

An alternative approach to calculating thermal conductivity is based on the Green-Kubo formula, which employs molecular dynamics simulations to calculate thermal currents over long time periods after thermal equilibrium is reached [20,21]. This technique takes into account high-order scattering processes, but the usage of semiempirical potentials leads to errors on the order of 50% [1].

The methods described above are unsuitable for rapid generation and screening of large databases of materials properties in order to identify trends and simple descriptors for thermal properties [22]. To accomplish this, we chose to implement a much cheaper approach, the "GIBBS" quasiharmonic Debye model [23]. This approach does not require large supercell calculations since it relies merely on first-principles calculations of the energy as a function of unit cell volume. It is thus much more tractable computationally and is eminently suited to investigating the thermal properties of entire classes of materials in a highly automated fashion, in order to identify promising candidates for more in-depth experimental and computational analysis. We incorporate this model in a new software library, the Automatic GIBBS Library (AGL), within the AFLOW [24–26] and Materials Project [27–29] frameworks

*On leave from the Department of Physics, NRCN, Israel.
†stefano@duke.edu

 ©2014 American Physical Society

for high-throughput computational materials science, and use it to construct a database of computed compound thermal conductivities and Debye temperatures.

II. THE AUTOMATIC GIBBS LIBRARY (AGL)

The AGL software library implements the "GIBBS" method [23] in the AFLOW [24–26] framework (C++ based framework) and the Materials Project [27–29] (Python implementation). The library includes automatic error handling and correction to facilitate high-throughput computation of materials thermal properties. The principal ingredients of the calculation are described in the following sections.

A. The GIBBS quasiharmonic Debye model

In thermodynamics, the equilibrium state of a system at a constant temperature and pressure minimizes its Gibbs free energy

$$G(\vec{x};p,T) = E(\vec{x}) + pV(\vec{x}) + A_{\rm vib}(\vec{x};T), \tag{1}$$

where $\vec{x}$ is a configuration vector containing all the information about the system's geometry, $E(\vec{x})$ is the total energy of the crystal (obtained, for example, from an electronic structure calculation), $A_{\rm vib}$ is the vibrational Helmholtz free energy, and p and $V(\vec{x})$ are the pressure and volume. It is assumed here that the electronic and intrinsic point defect contributions to the Helmholtz free energy is small, which is a good approximation for most materials at temperatures significantly below their melting point. In the quasiharmonic approximation, the Helmholtz vibrational energy is

$$A_{\rm vib}(\vec{x};T) = \int_0^\infty \left[\frac{\hbar\omega}{2} + k_B T\ \ln(1-e^{-\hbar\omega/k_B T})\right] \times g(\vec{x};\omega)d\omega, \tag{2}$$

where $g(\vec{x};\omega)$ is the phonon density of states. As mentioned before, calculation of the full phonon density of states is computationally demanding, requiring electronic structure calculations for multiple supercell configurations. Instead, the "GIBBS" method uses a quasiharmonic Debye model, where the Helmholtz free energy is expressed in terms of the Debye temperature $\theta_{\rm D}$:

$$A_{\rm vib}(\theta_D;T) = nk_BT\left[\frac{9}{8}\frac{\theta_{\rm D}}{T} + 3\ \ln(1-e^{-\theta_{\rm D}/T}) - D\left(\frac{\theta_{\rm D}}{T}\right)\right], \tag{3}$$

where n is the number of atoms in the unit cell and $D(\theta_{\rm D}/T)$ is the Debye integral

$$D(\theta_{\rm D}/T) = 3\left(\frac{T}{\theta_{\rm D}}\right)^3 \int_0^{\theta_{\rm D}/T} \frac{x^3}{e^x-1}dx. \tag{4}$$

TABLE I. Lattice thermal conductivity at 300 K, Debye temperature, and Grüneisen parameter of zinc-blende and diamond structure semiconductors. The values listed for $\theta^{\rm exp}$ are $\theta_{\rm a}$, except 141 K for HgTe, which is $\theta_{\rm D}$ [7]. Units: θ in K, κ in W/(m K).

Comp.	$\theta^{\rm exp}$	$\theta_{\rm a}^{\rm AGL}$	$\theta_{\rm D}^{\rm AGL}$	$\gamma^{\rm exp}$	$\gamma^{\rm AGL}$	$\kappa^{\rm exp}$	$\kappa^{\rm AGL}$
C	1450 [37,38]	1219	1536	0.75 [38]	1.74	3000 [38]	169.1
				0.9 [37]			
SiC	740 [37]	737	928	0.76 [37]	1.84	360 [41]	67.19
Si	395 [37,38]	451	568	1.06 [38]	2.09	166 [38]	20.58
				0.56 [37]			
Ge	235 [37,38]	235	296	1.06 [38]	2.3	65 [38]	6.44
				0.76 [37]			
BN	1200 [38]	1118	1409	0.7 [38]	1.73	760 [38]	138.38
BP	670 [37,38]	644	811	0.75 [38]	1.78	350 [38]	52.56
AlP	381 [38]	430	542	0.75 [38]	1.96	90 [42,43]	21.16
AlAs	270 [37,38]	300	378	0.66 [37,38]	2.04	98 [38]	12.03
AlSb	210 [37,38]	223	281	0.6 [37,38]	2.12	56 [38]	7.22
GaP	275 [37,38]	314	396	0.75 [38]	2.15	100 [38]	11.76
				0.76 [37]			
GaAs	220 [37,38]	240	302	0.75 [37,38]	2.23	45 [38]	7.2
GaSb	165 [37,38]	186	234	0.75 [37,38]	2.27	40 [38]	4.62
InP	220 [37,38]	241	304	0.6 [37,38]	2.22	93 [38]	7.78
InAs	165 [37,38]	195	246	0.57 [37,38]	2.26	30 [38]	5.36
InSb	135 [37,38]	158	199	0.56 [37,38]	2.3	20 [38]	3.64
						16.5 [7]	
ZnS	230 [37,38]	301	379	0.75 [37,38]	2.01	27 [38]	11.33
ZnSe	190 [37,38]	230	290	0.75 [37,38]	2.07	19 [38]	7.46
						33 [7]	
ZnTe	155 [37,38]	181	228	0.97 [37,38]	2.14	18 [38]	4.87
CdSe	130 [38]	186	234	0.6 [38]	2.19	4.4 [7]	4.99
CdTe	120 [37,38]	152	191	0.52 [37,38]	2.23	7.5 [38]	3.49
HgSe	110 [37]	151	190	0.17 [37]	2.4	3 [44]	3.22
HgTe	141 [7]	129	162	1.9 [7]	2.46	2.5 [7]	2.36
	100 [37]			0.46[37]			

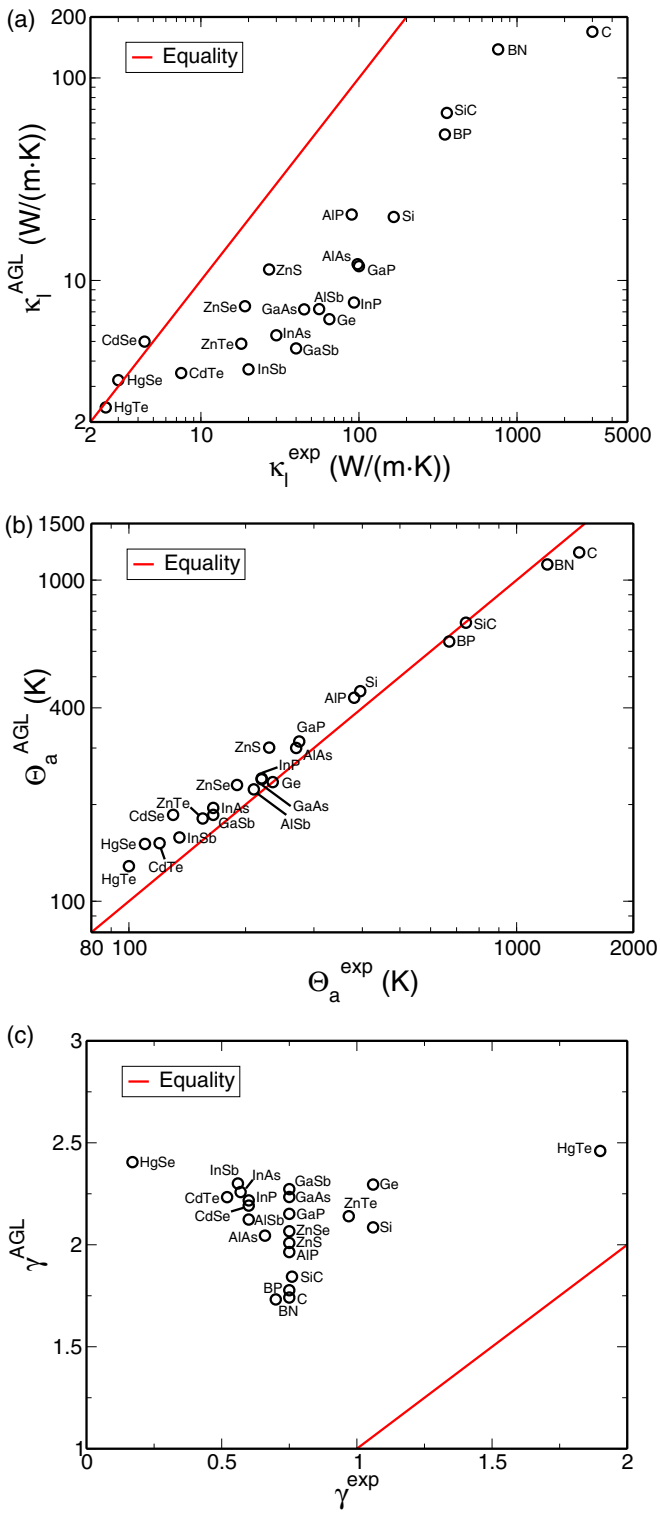

FIG. 1. (Color online) (a) Lattice thermal conductivity at 300 K, (b) acoustic Debye temperature, and (c) Grüneisen parameter of zinc-blende and diamond structure semiconductors.

In isotropic solids, changes in the geometry can be treated as isotropic changes in the volume, such that the magnitude of the configurational vector $\vec{x}$ is equal to the cube root of the volume; i.e., $x = V^{\frac{1}{3}}$. The value of θ_D can thus be calculated as [23,30,31]

$$\theta_D = \frac{\hbar}{k_B}[6\pi^2 V^{1/2} n]^{1/3} f(\sigma)\sqrt{\frac{B_S}{M}}. \tag{5}$$

Here, M is the mass of the unit cell, B_S is the adiabatic bulk modulus, and $f(\sigma)$ is given by

$$f(\sigma) = \left\{3\left[2\left(\frac{2}{3}\frac{1+\sigma}{1-2\sigma}\right)^{3/2} + \left(\frac{1}{3}\frac{1+\sigma}{1-\sigma}\right)^{3/2}\right]^{-1}\right\}^{\frac{1}{3}}, \tag{6}$$

in the assumption that the Poisson ratio σ is constant. The value of the Poisson ratio can be set as an input to AGL separately from the DFT calculations, e.g., to the experimentally measured value. For the calculations described in this paper this value is set at 0.25, which is the theoretical value for a Cauchy solid [23,31]. The Poisson ratio σ for crystalline materials is typically in the range of 0.2 to 0.3. Since the function $f(\sigma)$ behaves approximately linearly with values running from 0.9 to 0.7 when σ is in the range from 0.2 to 0.3, this approximation has only a small effect on the results. We have checked this by performing the AGL calculations using the literature values of the Poisson ratio where they are available. The correlation between calculated and experimental values of the thermal conductivity is typically within a few percent of that obtained with the constant value of 0.25.

The adiabatic bulk modulus, B_S, can be approximated by the zero-temperature limit of the isothermal compressibility (neglecting zero-point contributions), which we will refer to as B_{static}:

$$\begin{aligned} B_S &\approx B_{\text{static}}(\vec{x}) \approx B_{\text{static}}(\vec{x}_{\text{opt}}(V)) \\ &= V\left(\frac{\partial^2 E(\vec{x}_{\text{opt}}(V))}{\partial V^2}\right) = V\left(\frac{\partial^2 E(V)}{\partial V^2}\right), \end{aligned} \tag{7}$$

where $\vec{x}_{\text{opt}}$ is the configuration vector of the unit cell geometry. The Gibbs free energy of the system can be expressed as a function of the unit cell volume:

$$G(V;p,T) = E(V) + pV + A_{\text{vib}}(\theta_{\text{D}}(V);T), \tag{8}$$

where θ_D as a function of volume is evaluated from Eqs. (5) and (7), and $E(V)$ is obtained from a set of DFT calculations for unit cells with different volumes. Minimizing the Gibbs free energy with respect to volume, the equilibrium configuration at (p,T) is determined, and additional properties, including the equilibrium θ_{D}, bulk modulus, heat capacity, thermal coefficient of expansion, etc., can be evaluated.

B. Thermal calculation procedure

In order to calculate the thermal properties for a particular material with a particular structure, first a set of DFT (e.g., VASP [32]) calculations which only differ by isotropic variations in the unit cell volume are set up and run using the AFLOW or Materials Project framework. The resulting $E(V)$ is fitted by a polynomial, to calculate the adiabatic bulk modulus, B_S, as a function of volume from Eq. (7). The B_S values are then used to calculate the Debye temperature θ_{D} for each unit cell volume from Eq. (5). Next, the vibrational Helmholtz free energy $A_{\text{vib}}(\theta_{\text{D}}(V);T)$ as a function of volume is calculated using Eq. (3) for a given value of the temperature, T. The

TABLE II. Lattice thermal conductivity, Debye temperature, and Grüneisen parameter of rocksalt structure semiconductors. The values listed for θ^{exp} are θ_{a}, except 155 K for SnTe, which is θ_{D} [7]. Units: θ in K, κ in W/(m K).

Comp.	θ^{exp}	$\theta_{\text{a}}^{\text{AGL}}$	$\theta_{\text{D}}^{\text{AGL}}$	γ^{exp}	γ^{AGL}	κ^{exp}	κ^{AGL}
LiH	615 [37,38]	590	743	1.28 [37,38]	1.62	15 [38]	8.58
LiF	500 [37,38]	469	591	1.5 [37,38]	2.02	17.6 [38]	8.71
NaF	395 [37,38]	326	411	1.5 [37,38]	2.2	18.4 [38]	4.52
NaCl	220 [37,38]	225	284	1.56 [37,38]	2.23	7.1 [38]	2.43
NaBr	150 [37,38]	161	203	1.5 [37,38]	2.22	2.8 [38]	1.66
NaI	100 [37,38]	124	156	1.56 [37,38]	2.23	1.8 [38]	1.17
KF	235 [37,38]	242	305	1.52 [37,38]	2.29		2.68
KCl	172 [37,38]	175	220	1.45 [37,38]	2.38	7.1 [38]	1.4
KBr	117 [37,38]	131	165	1.45 [37,38]	2.37	3.4 [38]	1.0
KI	87 [37,38]	102	129	1.45 [37,38]	2.35	2.6 [38]	0.72
RbCl	124 [37,38]	133	168	1.45 [37,38]	2.34	2.8 [38]	1.09
RbBr	105 [37,38]	106	134	1.45 [37,38]	2.40	3.8 [38]	0.76
RbI	84 [37,38]	87	109	1.41 [37,38]	2.47	2.3 [38]	0.52
AgCl	124 [37]	187	235	1.9 [37]	2.5	1.0 [42,45]	2.58
MgO	600 [37,38]	602	758	1.44 [37,38]	1.95	60 [38]	31.86
CaO	450 [37,38]	459	578	1.57 [37,38]	2.07	27 [38]	19.54
SrO	270 [37,38]	317	399	1.52 [37,38]	2.09	12 [38]	12.47
BaO	183 [37,38]	242	305	1.5 [37,38]	2.09	2.3 [38]	8.88
PbS	115 [37,38]	179	226	2.0 [37,38]	2.02	2.9 [38]	6.48
PbSe	100 [38]	156	197	1.5 [38]	2.1	2.0 [38]	4.88
PbTe	105 [37,38]	135	170	1.45 [37,38]	2.04	2.5 [38]	4.15
SnTe	155 [7]	160	202	2.1 [7]	2.15	1.5 [7]	4.46

zero-pressure Gibbs free energy as a function of volume is then obtained by

$$G(\vec{x};0,T) = E(V) + A_{(\text{vib})}(\theta_{\text{D}}(V),T). \tag{9}$$

This Gibbs free energy is fitted by a polynomial which is minimized with respect to volume to find the equilibrium volume for any given value of T, at zero pressure. The polynomial is an expansion in $x = \sqrt[3]{V}$. Therefore, finite pressure can be added simply to the coefficient of the x^3 term. The volume which minimizes this modified polynomial for $G(p,V,T)$ is the equilibrium volume that gives the Gibbs free energy for each requested (p,T). This equilibrium volume is used to calculate the bulk modulus and Debye temperature of the material as a function of p and T, from Eqs. (7) and (5), respectively.

C. DFT calculation details

The DFT calculations to obtain $E(V)$ were performed using the VASP software [32] with projector-augmented-wave pseudopotentials [33] and the PBE parametrization of the generalized gradient approximation to the exchange-correlation functional [34]. The energies were calculated at zero temperature and pressure, with spin polarization and without zero-point motion or lattice vibrations. The initial crystal structures were fully relaxed (cell volume and shape and the basis atom coordinates inside the cell). An additional 100 different volume cells were calculated for each structure by increasing or decreasing the relaxed lattice parameter in fractional increments of 0.005. Numerical convergence to about 1 meV/atom was ensured by a high-energy cutoff (30% higher than the maximum cutoff of each of the potentials) and a 8000 k point Monkhorst-Pack [35] or Γ-centered (in the case of hexagonal unit cells) mesh.

D. The Grüneisen parameter

The Grüneisen parameter describes how the thermal properties of a material vary with the unit cell size. It is defined by the phonon frequencies dependence on the unit cell volume

$$\gamma_i = -\frac{V}{\omega_i}\frac{\partial \omega_i}{\partial V}. \tag{10}$$

Debye's theory assumes that all mode frequencies vary with the volume in the same ratio as the cutoff frequency (Debye frequency), so the Grüneisen parameter can be expressed in terms of θ_{D},

$$\gamma = -\frac{\partial\ \ln[\theta_D(V)]}{\partial\ \ln V}, \tag{11}$$

and calculated using the Mie-Grüneisen equation [31],

$$p - p_{T=0} = \gamma\frac{U_{\text{vib}}}{V}, \tag{12}$$

where U_{vib} is the vibrational internal energy,

$$U_{\text{vib}} = nk_BT\left[\frac{9}{8}\frac{\theta_D}{T} + 3D\left(\frac{\theta_D}{T}\right)\right]. \tag{13}$$

The expression in Eq. (10) can also be related to the macroscopic definition via a weighted average with the heat capacities for each branch of the phonon spectrum,

$$\gamma = \frac{\sum_i \gamma_i C_{V,i}}{\sum_i C_{V,i}}, \tag{14}$$

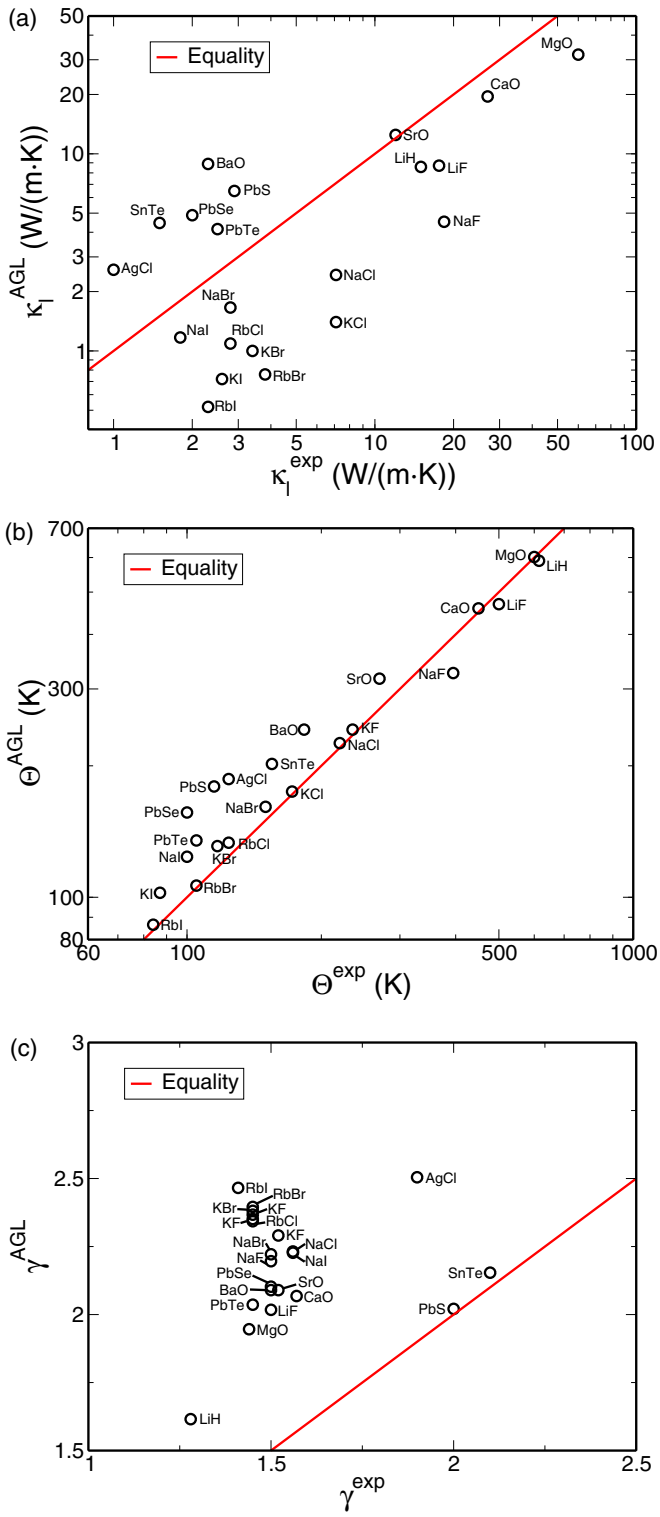

FIG. 2. (Color online) (a) Lattice thermal conductivity at 300 K, (b) Debye temperature, and (c) Grüneisen parameter of rocksalt structure semiconductors. The Debye temperatures plotted in (b) are θ_a, except for SnTe, where θ_D is quoted in Ref. [7].

which leads to the thermodynamic relations

$$\gamma = V\left(\frac{\partial P}{\partial E}\right)_V = \frac{\alpha B_S}{C_P \rho} = \frac{\alpha B_T}{C_V \rho}, \tag{15}$$

where ρ is the density of the material.

An alternative expression for the Grüneisen parameter was derived by Slater under the assumption of a constant Poisson ratio [36]

$$\gamma = -\frac{2}{3} - \frac{V}{2}\frac{d^2p/dV^2}{dp/dV}. \tag{16}$$

Equations (11), (12), and (16) have all been implemented within the AGL. Unless otherwise specified, the values of the Grüneisen parameter listed in the results and used to calculate the thermal conductivity are obtained using Eq. (12), as this is generally considered more accurate than Eq. (11) [23].

E. Thermal conductivity

In the AGL, the thermal conductivity is calculated by the method proposed by Slack [37,38] using the Debye temperature and the Grüneisen parameter:

$$\kappa_l(\theta_a) = \frac{0.849 \times 3\sqrt[3]{4}}{20\pi^3(1 - 0.514\gamma^{-1} + 0.228\gamma^{-2})} \times \left(\frac{k_B\theta_a}{\hbar}\right)^2 \frac{k_B m V^{\frac{1}{3}}}{\hbar\gamma^2}, \tag{17}$$

where V is the volume of the unit cell and m is the average atomic mass. It should be noted that the Debye temperature in this formula, θ_a, is slightly different than the traditional Debye temperature, θ_D, calculated in Eq. (5). Instead, θ_a is obtained by only considering the acoustic modes, based on the assumption that the optical phonon modes in crystals do not contribute to heat transport [37]. This θ_a is referred to as the "acoustic" Debye temperature [37,38]. It can be derived directly from the phonon DOS by integrating only over the acoustic modes [37,39]. Alternatively, it can be calculated from the traditional Debye temperature θ_D [37,38]

$$\theta_a = \theta_D n^{-\frac{1}{3}}. \tag{18}$$

To demonstrate the distinction between these two quantities, we include the values of both θ_D and θ_a, as calculated using AGL, in the tables of results in the following sections.

The thermal conductivity at temperatures other than θ_a is estimated by [37,38,40]

$$\kappa_l(T) = \kappa_l(\theta_a)\frac{\theta_a}{T}. \tag{19}$$

In principle, the Grüneisen parameter in Eq. (17) should also be derived only from the acoustic phonon modes [37]. However, unlike the case of θ_D and θ_a, there is no simple way to extract it from the traditional Grüneisen parameter. Instead, it must be calculated from Eq. (10) for each phonon branch separately and summed over the acoustic branches. This requires calculating the full phonon spectrum for different volumes, and is therefore too computationally demanding to be used for high-throughput screening. The dependence of the expression (17) on γ is weak [38]; thus the evaluation of κ_l using the traditional Grüneisen parameter introduces just a small systematic error which is insignificant for screening purposes.

F. Pearson and Spearman correlations

Pearson and Spearman correlations have been implemented separately from AGL, in order to analyze the results for entire

TABLE III. Lattice thermal conductivity at 300 K, Debye temperature, and Grüneisen parameter of wurzite structure semiconductors. The experimental Debye temperature values listed are θ_a, except 190 K for InSe [7] and 660 K for InN [41,46], which are θ_D. Units: θ in K, κ in W/(m K).

Comp.	θ^{exp}	θ_a^{AGL}	θ_D^{AGL}	γ^{exp}	γ^{AGL}	κ^{exp}	κ^{AGL}
SiC	740 [38]	586	930	0.75 [38]	1.86	490 [38]	42.49
AlN	620 [38]	554	880	0.7 [38]	1.85	350 [38]	36.73
GaN	390 [38]	373	592	0.7 [38]	2.07	210 [38]	18.17
ZnO	303 [38]	331	525	0.75 [38]	1.97	60 [38]	14.10
BeO	809 [38]	671	1065	1.38 [38,47,48]	1.76	370 [38]	39.26
				0.75 [38]			
CdS	135 [38]	181	287	0.75 [38]	2.14	16 [38]	4.40
InSe	190 [7]	115	230	1.2 [7]	2.24	6.9 [7]	1.84
InN	660 [41,46]	268	426	0.97 [46]	2.17	45 [41,46]	10.44

sets of materials. The Pearson correlation coefficient r is a measure of the linear correlation between two variables, X and Y. It is calculated by

$$r = \frac{\sum_{i=1}^{n}(X_i - \overline{X})(Y_i - \overline{Y})}{\sqrt{\sum_{i=1}^{n}(X_i - \overline{X})^2}\sqrt{\sum_{i=1}^{n}(Y_i - \overline{Y})^2}}, \tag{20}$$

where $\overline{X}$ and $\overline{Y}$ are the mean values of X and Y.

The Spearman rank correlation coefficient ρ is a measure of the monotonicity of the relation between two variables. The raw values of the two variables X_i and Y_i are sorted in ascending order, and are assigned rank values x_i and y_i which are equal to their position in the sorted list. If there is more than one variable with the same value, the average of the position values are assigned to each. The correlation coefficient is then given by

$$\rho = \frac{\sum_{i=1}^{n}(x_i - \overline{x})(y_i - \overline{y})}{\sqrt{\sum_{i=1}^{n}(x_i - \overline{x})^2}\sqrt{\sum_{i=1}^{n}(y_i - \overline{y})^2}}. \tag{21}$$

It is useful for determining how well the ranking order of the values of one variable predicts the ranking order of the values of the other variable.

III. RESULTS

We used the AGL to calculate the the Debye temperature, Grüneisen parameter, and thermal conductivity for a set of 75 materials with the diamond, zinc-blende, rocksalt, and wurzite structures, and 107 half-Heusler compounds. The results have been compared to first-principles calculations (and experimental values where available) of the half-Heusler compounds and to experimental values for the other structures.

A. Zinc-blende and diamond structure materials

Experimental values of thermal properties for materials with the zinc-blende [space group: $F\overline{4}3m$ (No. 216); Pearson symbol: $cF8$] and diamond [space group: $Fd\overline{3}m$ (No. 227); Pearson symbol: $cF8$] structures were published in Table II of Ref. [37] and Table 2.2 of Ref. [38]. They are shown with the calculated thermal conductivity at 300 K, the Debye temperature, and Grüneisen parameter for these materials in Table I and in Fig. 1. As shown in the table, for a few of these materials there are discrepancies in experimental values quoted in the different sources. For each entry we used the value from the most recent source for plotting the following figures and calculating the correlations reported here.

Comparison of the calculated and experimental results of Table I shows that the absolute agreement between them is quite poor, with discrepancies of tens, or even hundreds, of percent quite common. Considerable disagreements also exist between different experimental reports of these properties, in almost all cases where they exist. Unfortunately, the scarcity of experimental data from different sources on the thermal properties of these materials prevents reaching definite conclusions regarding the true values of these properties. The available data can thus only be considered as a rough indication of their order of magnitude.

Nevertheless, the Pearson correlation between the AGL calculated thermal conductivity values and the experimental values is high, 0.878. The Spearman correlation, 0.905, is even higher. The Spearman correlation between the experimental values of the thermal conductivity and θ_a as calculated with AGL is 0.925. There is also a strong correlation between the experimental values of θ_a and those calculated with AGL, with a Pearson correlation of 0.995 and a Spearman correlation of 0.984. The correlation for the Grüneisen parameter is much worse, with Pearson and Spearman correlations of 0.137 and −0.187, respectively.

Table 2.2 of Ref. [38] includes values of the thermal conductivity at 300 K, calculated using the experimental values of θ_a and γ. The Pearson correlation between these calculated thermal conductivity values and the experimental values is 0.932, and the corresponding Spearman correlation is 0.941. Both values are just slightly higher than the correlations we calculated using the AGL evaluations of θ_a and γ. Thus, the unsatisfactory quantitative reproduction of these quantities by the Debye quasiharmonic model has little impact on its effectiveness as a screening tool for high or low thermal conductivity materials. The model can be used when these experimental values are unavailable.

These results indicate that despite the quantitative disagreement between the calculated and experimental results for the thermal conductivity and θ_a, the AGL calculations are good indicators for the relative values of these quantities and for

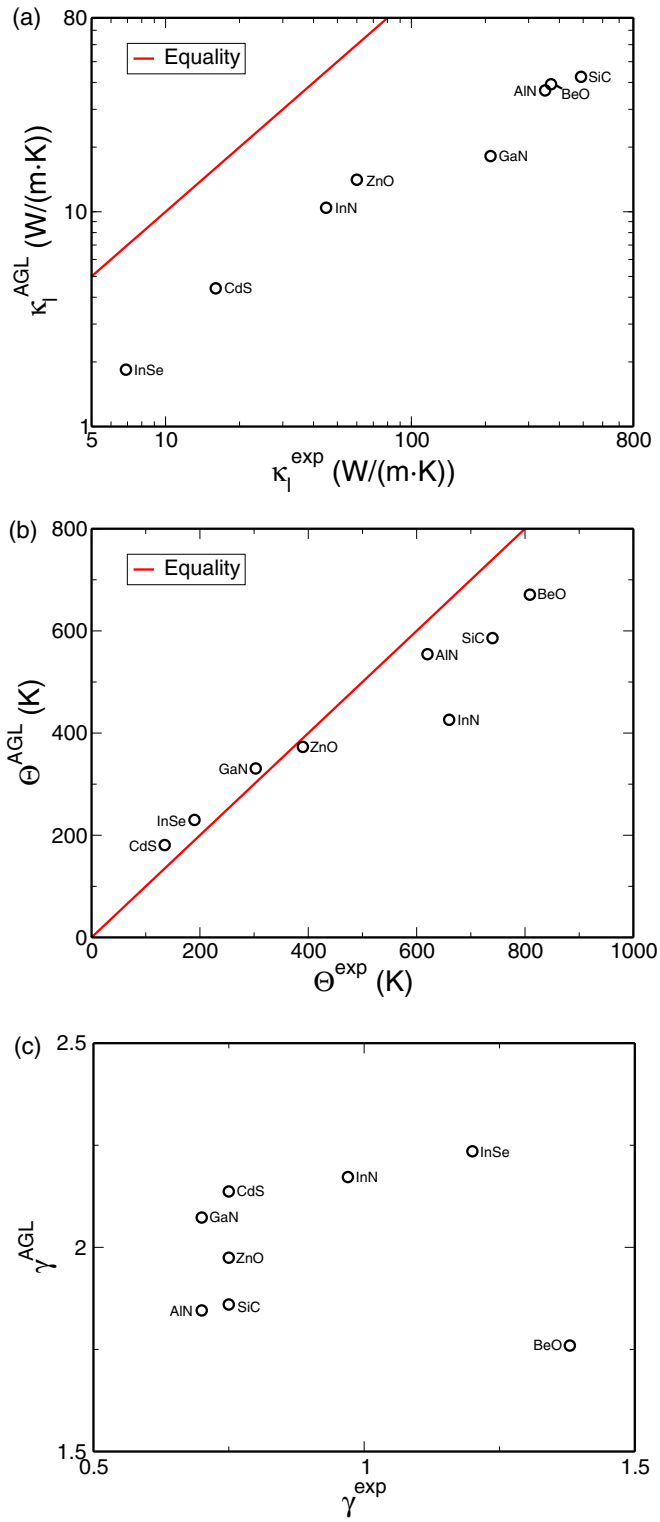

FIG. 3. (Color online) (a) Lattice thermal conductivity at 300 K, (b) Debye temperature, and (c) Grüneisen parameter of wurzite structure semiconductors. The Debye temperatures plotted in (b) are θ_a, except for InSe and InN, where θ_D values are quoted in Refs. [7,41,46].

ranking materials in order of increasing conductivity. For the diamond and zinc-blende structure materials, the calculated θ_a turns out to be a slightly better indicator of the ordinal order of the thermal conductivity than the calculated conductivity.

TABLE IV. Lattice thermal conductivity at 300 K, Debye temperature, and Grüneisen parameter of rhombohedral semiconductors. The experimental Debye temperatures are θ_D for Bi_2Te_3 and Sb_2Te_3, and θ_a for Al_2O_3. Units: θ in K, κ in W/(m K).

Comp.	θ^{exp}	θ_a^{AGL}	θ_D^{AGL}	γ^{exp}	γ^{AGL}	κ^{exp}	κ^{AGL}
Bi_2Te_3	155 [7]	112	191	1.49 [7]	2.13	1.6 [7]	2.79
Sb_2Te_3	160 [7]	127	217	1.49 [7]	2.2	2.4 [7]	2.90
Al_2O_3	390 [37]	430	927	1.32 [37]	1.91	30 [49]	20.21
Cr_2O_3		340	733		2.26	16 [42,50]	10.87
Fe_2O_3		235	506		5.32	11.3 [42,51]	0.60
Bi_2Se_3		130	223		2.08	1.34 [42]	3.60

B. Rocksalt structure materials

Experimental values of the thermal properties of materials with the rocksalt structure [space group: $Fm\bar{3}m$ (No. 225); Pearson symbol: $cF8$] were published in Table III of Ref. [37] and Table 2.1 of Ref. [38]. They are compared to the values calculated by the AGL in Table II and Fig. 2. As was the case for the zinc-blende structure materials, we have included the AGL results for both θ_D and θ_a in the table. The experimental values listed in the table are all for θ_a [38], with the exception of the value of 155 K for SnTe, which is for θ_D[7]. The AGL θ_a values were used for plotting and correlation calculations, with the exception of that for SnTe, where θ_D was used for plotting Fig. 2(b) and for calculating the correlation between the Debye temperatures.

The Pearson correlation between the calculated and experimental values for the thermal conductivity is 0.910. The Spearman correlation is 0.445. The Spearman correlation between the experimental values of the thermal conductivity and the calculated values of θ_a is 0.645. The Pearson correlation between the calculated and experimental values for the Debye temperature is 0.982 and the corresponding Spearman correlation is 0.948. The correlation for the Grüneisen parameter is much worse, with Pearson and Spearman correlations of 0.118 and −0.064, respectively.

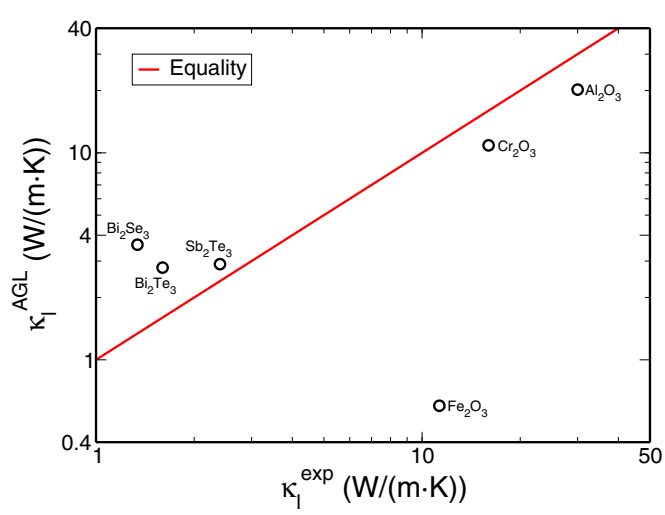

FIG. 4. (Color online) Lattice thermal conductivity of rhombohedral semiconductors at 300 K.

TABLE V. Lattice thermal conductivity at 300 K, Debye temperature, and Grüneisen parameter of body-centered tetragonal semiconductors. Units: θ in K, κ in W/(m K).

Comp.	θ_D^{exp}	θ_a^{AGL}	θ_D^{AGL}	γ^{exp}	γ^{AGL}	κ^{exp}	κ^{AGL}
$CuGaTe_2$	226 [7]	117	234	1.46 [7]	2.32	2.2 [7]	1.77
$ZnGeP_2$	500 [42]	195	390		2.13	35 [42,52]	4.45
						36 [42,52]	
						18 [42,53,54]	
$ZnSiAs_2$	347 [42,55]	171	342		2.15	14 [42,53,54]	3.70
$CuInTe_2$	185 [42,56]	108	215	0.93 [56]	2.33	10 [42,56]	1.55
	195 [42,57]						
$AgGaS_2$	255 [42,58]	162	324		2.20	1.4 [42,52]	2.97
						1.5 [42,52]	
$CdGeP_2$	340 [42,58]	168	335		2.20	11 [42,53,54]	3.40
$CdGeAs_2$		133	266		2.20	42 [42,53]	2.44
$CuGaS_2$	356 [42,58]	194	387		2.24	5.09 [42]	3.78
$CuGaSe_2$	262 [42,57]	147	294		2.27	12.9 [42,56]	2.54
$ZnGeAs_2$		150	299		2.16	11 [42,53]	2.95

Table 2.1 of Ref. [38] includes values of the thermal conductivity at 300 K, calculated using the experimental values of θ_a and γ. The Pearson correlation between these calculated thermal conductivities and their experimental values is 0.986, and the corresponding Spearman correlation is 0.761. Comparing these values with the correlations obtained using the AGL calculated quantities, we find that the latter are more significantly degraded than for the diamond and zinc-blende structures. This is despite the similar correlations obtained for θ_a and γ in these two cases. Nevertheless, the Pearson correlation between the calculated and experimental conductivities is high in both calculations, indicating that the AGL approach may be used as a screening tool for high-conductivity compounds in cases where gaps exist in the experimental data for these materials.

C. Wurzite structure materials

Experimental results for wurzite structure materials [space group: $P6_3mc$ (No. 186); Pearson symbol: $hP4$] appear in Table 2.3 of Ref. [38]. Their comparison with our calculation results is shown in Table III and Fig. 3. As was the case for the zinc-blende and wurzite structure materials, we have included the AGL results for both θ_D and θ_a in the table, while the AGL θ_a was used for plotting Fig. 3 and calculating the correlations. The experimental values listed in the table are all for θ_a [38], with the exceptions of the values of 190 K for InSe [7] and 660 K for InN [41,46], which are for θ_D. The AGL θ_a values were used for plotting and correlation calculations, with the exception of those for InSe and InN, where θ_D was used for plotting Fig. 3(b) and for calculating the correlation between the Debye temperatures.

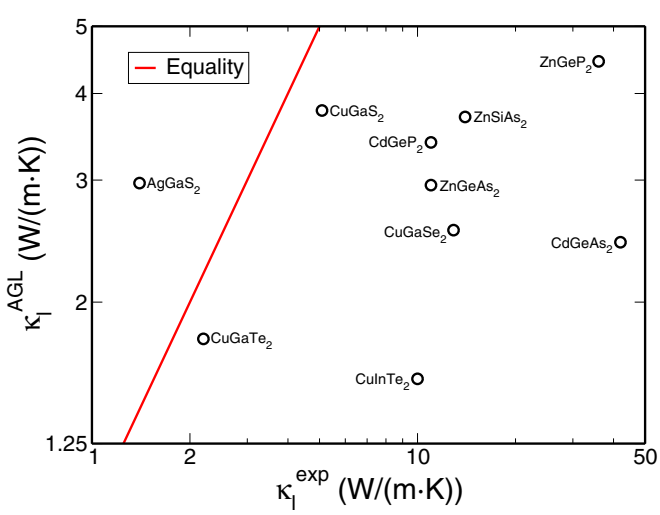

FIG. 5. (Color online) Lattice thermal conductivity of body-centered tetragonal semiconductors at 300 K.

The Pearson correlation between the AGL thermal conductivity values and the experimental values is 0.977. The corresponding Spearman correlation is 1.0. The Spearman correlation between the experimental values of the thermal conductivity and the calculated values of θ_a is 0.976. The Pearson correlation between the experimental and calculated values of the Debye temperature is 0.960, and the corresponding Spearman correlation is 0.976. The correlations for the Grüneisen parameter are both poor, with Pearson and Spearman values of −0.039 and 0.160, respectively.

Table 2.3 of Ref. [38] includes values of the thermal conductivity at 300 K, calculated using the experimental values of the Debye temperature and Grüneisen parameter. The Pearson correlation between these calculated thermal conductivity values and the experimental values is 0.996, and the corresponding Spearman correlation is 1.0. These values are again higher than the correlations obtained using the AGL calculated quantities; however, all of these correlations are very high so either of the calculation methods could serve as a reliable screening tool of the thermal conductivity. It should be noted that the high correlations calculated with the experimental θ_a and γ were obtained using $\gamma = 0.75$ for BeO. Table 2.3 of Ref. [38] also cites an alternative value of $\gamma = 1.38$ for BeO (Table III). Using this outlier value would severely degrade the results down to 0.7, for the Pearson correlation, and 0.829, for the Spearman correlation. These values are too low for a reliable screening tool. This demonstrates the ability of the AGL calculations to compensate for anomalies in the experimental data when they exist and

TABLE VI. Lattice thermal conductivity at 300 K, Debye temperature, and Grüneisen parameter of materials with various structures at 300 K. The experimental Debye temperatures are θ_D, except ZnSb, for which it is θ_a. Units: θ in K, κ in W/(m K).

Comp.	Pearson	θ^{exp}	θ_a^{AGL}	θ_D^{AGL}	γ^{exp}	γ^{AGL}	κ^{exp}	κ^{AGL}
$CoSb_3$	$cI32$	307 [7]	113	284	0.95 [7]	2.63	10 [7]	1.60
$IrSb_3$	$cI32$	308 [7]	112	283	1.42 [7]	2.34	16 [7]	2.64
ZnSb	$oP16$	92 [40]	97	244	0.76 [40]	2.24	3.5 [40,59]	1.24
Sb_2O_3	$oP20$		154	418		2.13	0.4 [42]	3.45
InTe	$cP2$	186 [7]	152	191	1.0 [7]	2.28	1.7 [7]	3.12
Bi_2O_3	$mP20$		127	345		2.1	0.8 [42]	3.04
SnO_2	$tP6$		298	541		2.48	98[60]	9.56
							55 [60]	

still provide a reliable screening method for the thermal conductivity.

D. Rhombohedral materials

Experimental results for rhombohedral materials [space groups: $R\bar{3}mR$ (No. 166), $R\bar{3}mH$ (No. 166), and $R\bar{3}cH$ (No. 167); Pearson symbols: $hR5$, $hR10$] are compared to the results of our calculations in Table IV and Fig. 4. The experimental Debye temperatures are for θ_D in the case of Bi_2Te_3 and Sb_2Te_3, and for θ_a in the case of Al_2O_3. The Pearson correlation between the experimental and calculated thermal conductivity values is 0.893. The corresponding Spearman correlation is 0.486. The Spearman correlation between the experimental values of the thermal conductivity and the values of θ_a calculated with AGL is 0.829.

The thermal conductivity of Fe_2O_3 is a clear outlier in this data set (see Fig. 4). Its Grüneisen parameter, calculated with Eq. (12), is 5.32. It is abnormally high. Equation (11) gives a similar value of 5.36, whereas Eq. (16) gives a lower, but still very high, value of 4.06. Ignoring Fe_2O_3 in the comparison increases the Pearson correlation of the calculated and experimental values of the thermal conductivity to 0.997, while the Spearman correlation increases to 0.7.

TABLE VII. Thermal conductivities of half-Heusler semiconductors at 300 K compared to full anharmonic phonon *ab initio* parametrization from Ref. [2]. Units: θ in K, κ in W/(m K).

Comp.	θ_a^{AGL}	θ_D^{AGL}	γ^{AGL}	κ^{anh} [2]	κ^{AGL}
AgKTe	105	152	2.26	0.508	1.0
BeNaP	302	436	2.05	4.08	5.3
BiBaK	95	137	1.94	2.19	1.59
BiKSr	99	143	1.96	1.96	1.45
BiLiSr	126	182	1.94	3.04	2.48
CoAsZr	306	442	2.14	24.0	17.51
CoBiHf	204	294	2.17	18.6	10.43
CoSbZr	231	333	3.00	25.0	4.69
CoScSe	230	331	2.09	15.0	6.64
CoSiTa	296	427	1.92	37.8	23.06
FeNbP	343	495	1.94	109.0	23.79
GeCaZn	197	284	2.05	2.75	4.53
GeNaY	189	273	2.04	8.06	4.28
LiBaSr	88	127	1.30	0.582	1.84
IrPTi	309	446	2.18	27.4	20.25
NiPbTi	205	296	2.20	109.0	7.35
NiSbSc	232	334	2.03	19.5	9.13
NiSnTi	249	359	2.06	17.9	10.7
NiSnZr	229	330	2.06	19.6	10.22
OsSbTa	227	328	2.14	29.6	16.62
PdAsY	230	332	2.17	5.48	9.43
PdSrTe	130	188	2.13	1.16	2.44
PtGaTa	242	349	2.19	32.9	16.78
PtGeTi	263	379	2.23	16.9	14.41
PtLaNb	140	202	2.69	16.5	2.2
RhHfSb	232	335	2.18	21.8	14.06
RhNbSi	345	497	2.09	15.3	26.15
RuAsV	334	482	2.19	23.5	21.37
SbCaK	141	203	1.92	2.70	2.47
SiCdSr	168	242	2.05	13.5	3.79
SnBaSr	114	165	1.71	2.01	3.19
TeAgLi	166	239	2.32	1.52	2.79

E. Body-centered tetragonal materials

Results for a set of body-centered tetragonal materials [space group: $I\bar{4}2d$ (No. 122); Pearson symbol: $tI16$] are shown in Table V and in Fig. 5. For the materials $ZnGeP_2$

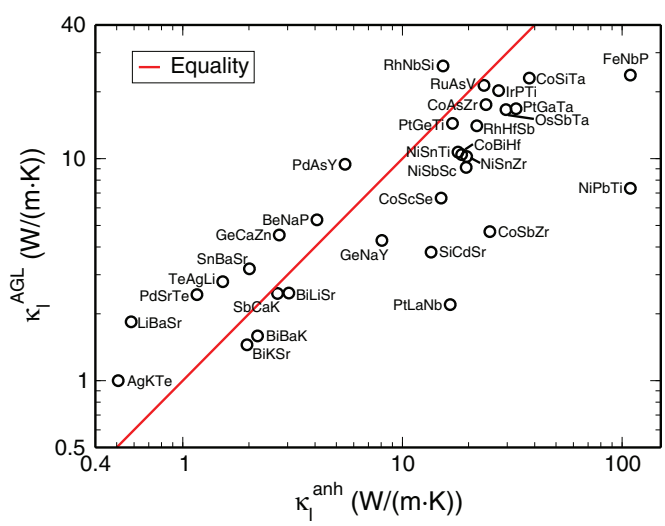

FIG. 6. (Color online) Thermal conductivities of half-Heusler semiconductors at 300 K compared to full anharmonic phonon *ab initio* parametrization from Ref. [2].

TABLE VIII. Thermal conductivities of half-Heusler semiconductors at 300 K compared to machine learning algorithm predictions from Ref. [2]. Units: θ in K, κ in W/(m K).

Comp.	θ_a^{AGL}	θ_D^{AGL}	γ^{AGL}	κ^{ML} [2]	κ^{AGL}	Comp.	θ_a^{AGL}	θ_D^{AGL}	γ^{AGL}	κ^{ML} [2]	κ^{AGL}
AuAlHf	217	313	2.12	16.7	12.14	NiBiSc	207	299	2.17	14.3	7.8
BLiSi	433	624	2.07	62.1	9.39	NiBiY	187	269	2.16	10.6	6.8
BiBaK	95	137	1.94	1.24	1.59	NiGaNb	289	417	2.11	22.9	14.79
CoAsHf	266	383	2.13	20.0	15.76	NiGeHf	238	343	2.02	19.6	13.05
CoAsTi	345	497	2.15	37.1	18.96	NiGeTi	330	476	2.10	25.3	17.56
CoAsZr	306	442	2.14	27.7	17.51	NiGeZr	295	426	2.07	21.1	16.78
CoBiHf	204	294	2.17	22.5	10.43	NiHfSn	230	332	2.08	19.5	12.97
CoBiTi	236	341	2.19	27.1	11.02	NiPbZr	195	281	2.19	15.2	7.5
CoBiZr	223	322	2.17	17.8	11.14	NiSnTi	249	359	2.06	16.8	10.7
CoGeNb	295	425	2.39	36.2	12.12	NiSnZr	229	330	2.06	17.5	10.22
CoGeTa	266	383	2.24	27.2	14.19	OsNbSb	254	367	2.12	24.8	19.38
CoGeV	334	482	2.01	29.1	20.26	OsSbTa	227	328	2.14	28.8	16.62
CoHfSb	190	274	1.69	21.9	12.18	PCdBa	198	285	2.24	6.05	3.45
CoNbSi	323	466	2.18	30.1	15.65	PdBiSc	194	280	2.23	9.95	7.22
CoNbSn	238	343	2.56	20.7	7.08	PdGeZr	267	385	2.18	18.2	14.04
CoSbTi	263	379	2.10	23.3	12.13	PdHfSn	218	314	2.21	15.1	11.35
CoSbZr	231	333	3.0	24.4	4.69	PdPbZr	203	293	2.29	10.3	8.72
CoSiTa	296	427	1.92	36.9	23.06	PtGaTa	242	349	2.19	32.3	16.78
CoSnTa	217	313	2.32	22.7	8.77	PtGeTi	263	379	2.23	26.7	14.41
CoSnV	266	383	2.49	19.8	8.47	PtGeZr	245	354	2.19	15.9	14.39
FeAsNb	339	489	2.13	47.6	23.09	PtLaSb	168	243	2.11	1.72	7.05
FeAsTa	295	425	2.13	32.9	21.08	RhAsTi	311	449	2.18	33.1	17.74
FeGeW	245	354	1.40	32.8	31.56	RhAsZr	284	409	2.17	27.1	16.73
FeNbSb	216	311	1.79	29.1	11.63	RhBiHf	182	263	2.25	12.8	8.01
FeSbTa	196	282	1.65	31.2	13.59	RhBiTi	228	329	2.25	13.0	11.1
FeSbV	305	440	1.50	24.1	39.0	RhBiZr	218	314	2.22	13.0	11.43
FeTeTi	266	384	2.24	26.2	11.02	RhLaTe	195	281	2.24	2.84	7.69
GeAlLi	270	390	2.06	16.5	6.36	RhNbSn	275	396	2.19	15.7	17.67
IrAsTi	277	399	2.22	30.1	16.92	RhSnTa	227	327	2.18	20.3	12.98
IrAsZr	255	368	2.19	17.4	16.04	RuAsNb	306	442	2.17	43.7	20.59
IrBiZr	206	297	2.24	12.8	11.67	RuAsTa	279	402	2.19	33.4	20.21
IrGeNb	279	402	2.17	33.0	20.88	RuNbSb	284	409	2.17	22.7	19.91
IrGeTa	256	369	2.15	37.2	20.43	RuSbTa	239	344	2.15	20.9	15.58
IrGeV	288	416	2.19	30.0	19.34	RuTeZr	241	348	2.26	21.3	11.76
IrHfSb	221	319	2.20	24.7	14.66	SbNaSr	139	200	1.90	3.49	2.83
IrNbSn	232	334	2.18	19.8	13.93	SiAlLi	363	523	2.02	20.9	9.26
IrSnTa	218	314	2.23	22.1	13.42	ZnLiSb	176	254	2.12	6.44	3.09
NiAsSc	300	432	2.11	17.5	13.32						

and $AgGaS_2$ there are three and two experimental values listed for κ^{exp}. This is due to the materials having different thermal conductivities in different crystalline directions [52]. The following results were obtained for the direction parallel to the optic axis, 36 W/(m K) and 1.4 W/(m K) for $ZnGeP_2$ and $AgGaS_2$, respectively. All of the experimental Debye temperatures listed in the table are the traditional Debye temperatures, θ_D.

The Pearson correlation between the AGL thermal conductivity values and the experimental values is 0.265. The corresponding Spearman correlation is 0.201. The Spearman correlation between the experimental values of the thermal conductivity and the calculated values of θ_a is 0.201. The low correlations for this set of materials are due to their anisotropic structure, where the materials display different thermal conductivities along different lattice directions. This demonstrates the limits of the isotropic approximation made in the GIBBS method.

F. Miscellaneous materials

The results for materials with various other structures are shown in Table VI. The materials are $CoSb_3$ and $IrSb_3$ [space group: $Im\bar{3}$ (No. 204); Pearson symbol: $cI32$], ZnSb [space group: $Pbca$ (No. 61); Pearson symbol: $oP16$], Sb_2O_3 [space group: $Pccn$ (No. 56); Pearson symbol: $oP20$], InTe [space group: $Pm\bar{3}m$ (No. 221); Pearson symbol: $cP2$], Bi_2O_3 [space group: $P121/c1$ (No. 14); Pearson symbol: $mP20$], and SnO_2 [space group: $P42/mnm$ (No. 136); Pearson symbol: $tP6$]. The experimental Debye temperatures listed in the table are the traditional Debye temperatures, θ_D, with the exception of ZnSb for which it is θ_a.

For these materials, the Pearson correlation between the calculated and experimental values of the thermal conductivity is 0.927. The corresponding Spearman correlation is −0.071. The Spearman correlation between the experimental values of the thermal conductivity and the calculated values of θ_a is −0.107.

The low correlation values, particularly for the Spearman correlation, for this set of materials demonstrates the importance of the information about the material structure as an input for the AGL method. This is partly due to the fact that the Grüneisen parameter tends not to vary significantly between materials with a particular structure, thus reducing its effect on the ordinal ranking of the thermal conductivity of materials with the same structure.

G. Half-Heusler materials

Carrete *et al.* [2,61] studied the thermal conductivity of 107 half-Heusler [space group: $F\bar{4}3m$ (No. 216); Pearson symbol: $cF12$] compounds with *ab initio* and machine learning techniques. In this section we compare their results with our AGL calculations. We first consider a subset of these half-Heusler materials, taken from Table I of Ref. [2], for which the thermal conductivity values were calculated using full anharmonic phonon parametrization solutions of the BTE. The thermal conductivities at 300 K for this set of materials as calculated with Eq. (19) are shown in Table VII and in Fig. 6. The Pearson correlation between the AGL thermal conductivity values and the full anharmonic phonon calculations is 0.495. The corresponding Spearman correlation is 0.810. The Spearman correlation between the full anharmonic phonon calculation values of the thermal conductivity and the values of θ_a as calculated with AGL is 0.730. A major contributor to the low Pearson correlation is the outlier calculated value of the thermal conductivity of FeNbP and NiPbTi, 109.0 W/(m K) [2]. If these materials are removed from the data set, the Pearson correlation increases to 0.782.

The second subset of half-Heusler materials studied is taken from Table III of Ref. [2], where the thermal conductivity was estimated using a machine learning algorithm. Comparison of these values with the thermal conductivity at 300 K calculated with Eq. (19) is shown in Table VIII and Fig. 7. The Pearson correlation between the AGL thermal conductivities and those produced by the machine learning algorithm is 0.578. The corresponding Spearman correlation is 0.706. The Spearman correlation between the machine learning thermal conductivities and the AGL values of θ_a is 0.679.

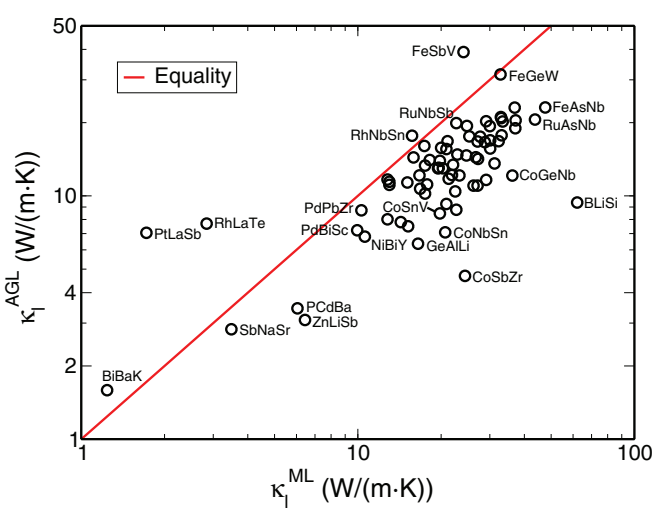

FIG. 7. (Color online) Thermal conductivities of half-Heusler semiconductors at 300 K compared to machine learning algorithm predictions from Ref. [2].

TABLE IX. Thermal conductivities of half-Heusler semiconductors at 300 K compared to experimental values. Units: θ in K, κ in W/(m K).

Comp.	θ_a^{AGL}	θ_D^{AGL}	γ^{AGL}	κ^{ML} [2]	κ^{AGL}	κ^{exp}
CoHfSb	190	274	1.69	21.9	12.18	17 [62]
CoSbTi	263	379	2.10	23.3	12.13	12 [63]
						25 [64]
CoSbZr	231	333	3.0	24.4	4.69	15 [64]
FeSbV	305	440	1.50	24.1	39.0	13 [65]
NiHfSn	230	332	2.08	19.5	12.97	6.7 [66]
NiSnTi	249	359	2.06	16.8	10.7	9.3 [66]
NiSnZr	229	330	2.06	17.5	10.22	8.8 [66]
						17.2 [67]

Experimental results for the thermal conductivity of 7 of these half-Heusler materials were available in the literature, and these values are shown in Table IX and Fig. 8. The Pearson correlation between the AGL thermal conductivities and the experimental values is 0.064, while the corresponding Spearman correlation is −0.036. The Spearman correlation between the experimental thermal conductivities and the AGL values of θ_a is 0.0. However, this is a small sample set, and these low correlation values appear to be primarily due to the outlier material CoSbZr, for which AGL predicts a relatively high value of 3.0 for the Grüneisen parameter. Ignoring this material in the comparison increases the Pearson correlation between the thermal conductivities to 0.262 and the Spearman correlation to 0.314.

H. AGL predictions for zinc-blende materials

In order to demonstrate the potential utility of the AGL method for high-throughput screening of the thermal properties of materials we have calculated the Debye temperature, Grüneisen parameter, and thermal conductivity for 45 zinc-blende structure [space group: $F\bar{4}3m$ (No. 216); Pearson

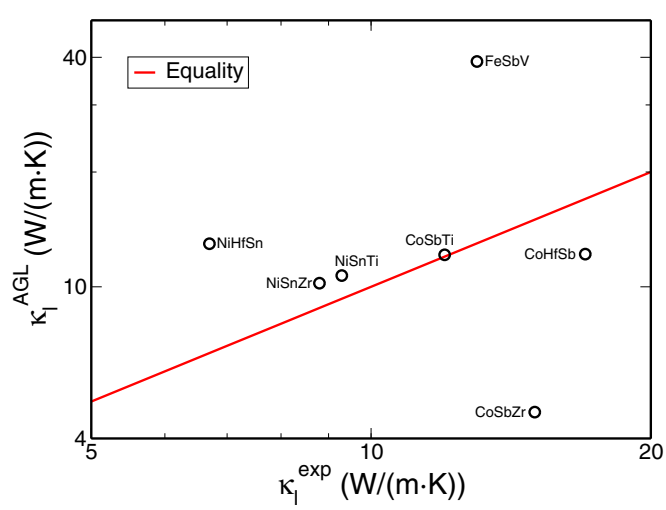

FIG. 8. (Color online) Thermal conductivities of half-Heusler semiconductors at 300 K compared to experimental measurements.

TABLE X. Lattice thermal conductivity at 300 K, Debye temperature, and Grüneisen parameter of zinc-blende structure materials for which the experimental thermal conductivity is not available in the literature. Units: θ in K, κ in W/(m K).

Comp.	θ_a^{AGL}	θ_D^{AGL}	γ^{AGL}	κ^{AGL}	Comp.	θ_a^{AGL}	θ_D^{AGL}	γ^{AGL}	κ^{AGL}
AgI	123	155	2.45	1.51	MgSe	250	315	1.91	8.51
AgO	247	311	2.06	7.19	MgTe	187	236	1.94	5.57
AgSe	179	225	2.52	3.09	MoN	447	563	1.82	45.92
AuN	259	326	2.49	9.03	NbN	493	621	1.97	50.62
BAs	420	529	1.95	25.75	NiN	416	524	1.58	30.30
BeO	845	1065	1.74	62.77	PdN	387	487	2.37	18.2
BeS	506	637	1.76	27.54	PrN	309	389	1.27	58.21
BeSe	324	408	1.80	15.6	ReN	385	485	1.83	51.39
BeTe	237	299	1.85	9.77	RhN	450	567	2.27	29.91
CaSe	208	262	1.84	6.78	RuN	487	614	2.18	40.49
CdS	228	287	2.15	6.91	SbSn	143	180	1.70	5.52
CoO	427	538	2.41	14.46	ScSi	298	375	1.78	12.41
CuBr	190	239	2.44	2.94	ScSn	177	223	1.85	5.85
CuCl	234	295	2.40	3.76	SiP	357	450	2.97	4.90
CuF	272	343	2.34	4.66	TaN	379	477	1.97	41.64
CuI	161	203	2.48	2.45	TcB	371	468	1.59	35.46
GaBi	140	177	2.18	3.32	TcN	469	591	2.43	28.08
GdO	275	346	1.92	16.84	TiB	448	565	1.69	31.06
GeP	239	301	1.54	11.5	WN	344	433	2.44	19.76
GeSc	231	291	1.88	8.41	YN	373	470	1.80	28.51
HfN	348	439	1.89	36.14	ZnO	417	525	1.95	22.38
HgS	176	222	2.34	4.35	ZrN	450	567	1.92	41.65
IrN	371	467	2.19	31.79					

symbol: $cF8$] materials which were not included in Table I, and for which experimental values of the thermal conductivity do not seem to be available in the literature. The results for these materials are shown in Table X and in Fig. 9.

From these results, it is noticeable that BeO is predicted to have the highest thermal conductivity, with a value similar to that of SiC. This high thermal conductivity is in agreement with recent first-principles calculations [68]. Another set of materials predicted to have high thermal conductivity includes the nitrides PrN, ReN, NbN, and MoN. Although BAs was previously predicted to have an extremely high thermal conductivity [15], the AGL value is only slightly higher than that of Si or AlP, and less than that of BP, BN, or SiC. The materials with the lowest thermal conductivity in this set are AgI and CuI. AgI, in particular, is predicted by AGL to have a thermal conductivity lower than that of any of the materials in Table I.

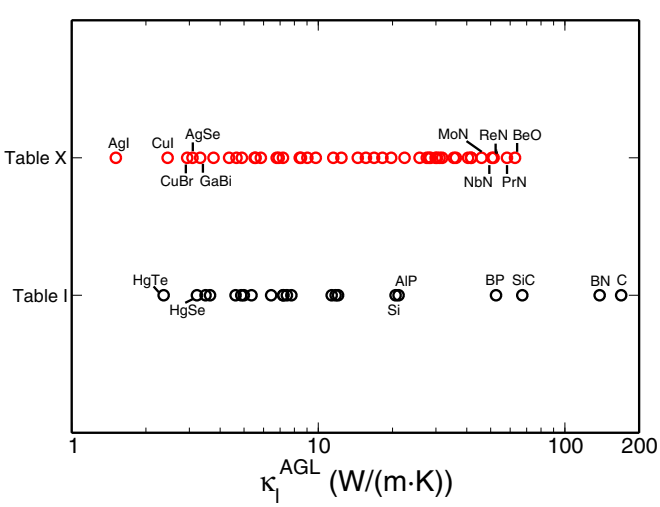

FIG. 9. (Color online) Predicted thermal conductivities of zinc-blende structure materials at 300 K. The AGL values for the materials with experimental data listed in Table I are shown in black (see also Fig. 1). AGL predictions for materials with no experimental data are in red.

IV. CONCLUSIONS

We implemented the "GIBBS" quasiharmonic Debye model in the AGL software package within the AFLOW and Materials Project high-throughput computational materials science frameworks. We used it to automatically calculate the thermal conductivity, Debye temperature, and Grüneisen coefficient of materials with various structures and compared them with experimental results.

A major aim of high-throughput calculations is to identify useful markers (descriptors) for screening large data sets of structures for desirable properties [22]. In this study we examined whether the *inexpensive-to-calculate* Debye model thermal properties may be useful as such markers for high thermal conductivity materials, despite the well-known deficiencies of this model in their quantitative evaluation. We therefore concentrated on correlations between the calculated quantities and the corresponding experimental data.

The correlations between the experimental values of the thermal conductivity and those calculated with AGL are summarized in Table XI. For the entire set of materials examined we find a high Pearson correlation of 0.880 between κ^{exp} and κ^{AGL}. It is particularly high, above 0.9, for materials with

TABLE XI. Summary of correlations between experimental and AGL lattice thermal conductivity values. The total value is for the set containing all of the non-half-Heusler materials.

Comp. set	Pearson $\kappa^{exp} \leftrightarrow \kappa^{AGL}$	Spearman $\kappa^{exp} \leftrightarrow \kappa^{AGL}$	Spearman $\kappa^{exp} \leftrightarrow \theta_a^{AGL}$
Zinc blende	0.878	0.905	0.925
Rocksalt	0.910	0.445	0.645
Wurzite	0.977	1.0	0.976
Rhombohedral	0.893	0.486	0.829
Tetragonal	0.265	0.201	0.201
Misc.	0.927	−0.071	−0.107
Total	0.880	0.734	0.752

high-symmetry (cubic or rhombohedral) structures, but significantly lower for anisotropic materials. We also compared these results with similar calculations of the thermal conductivity, using the experimental values of the Debye temperature and Grüneisen coefficient. The two methods gave similar Pearson correlations for the thermal conductivities, demonstrating that the AGL approach can rectify the lack of this experimental data in screening large data sets of materials.

The Spearman correlation between κ^{exp} and θ^{AGL} for the entire set of materials is almost as high as the Pearson correlation between the calculated and experimental conductivities. It is, however, less consistent for the high-symmetry structures, with a relatively low value of 0.645 for the rocksalt structures. The Spearman correlation between κ^{exp} and κ^{AGL} is found to be inferior to both previous measures as a descriptor of high-conductivity materials. The correlations for the half-Heusler materials are summarized in Table XII.

TABLE XII. Summary of correlations between *ab initio* and AGL lattice thermal conductivity values for the half-Heusler materials.

Comp. set	Pearson $\kappa^{anh} \leftrightarrow \kappa^{AGL}$	Spearman $\kappa^{anh} \leftrightarrow \kappa^{AGL}$	Spearman $\kappa^{anh} \leftrightarrow \theta_a^{AGL}$
Full anharmonic	0.495	0.810	0.730
Machine learning	0.578	0.706	0.679

Overall, despite the quantitative limitations of the method, the AGL approach can be useful for quickly screening large data sets of materials for favorable thermal properties.

ACKNOWLEDGMENTS

We thank Jesus Carrete, Natalio Mingo, Gus Hart, Anubhav Jain, Shyue Ping Ong, Kristin Persson, and Gerbrand Ceder for various technical discussions. We acknowledge support by the DOE (DE-AC02-05CH11231), specifically the Basic Energy Sciences program under Grant No. EDCBEE. The consortium AFLOWLIB.org acknowledges Duke University Center for Materials Genomics and the Cray corporation for computational support.

[1] M. Zebarjadi, K. Esfarjani, M. S. Dresselhaus, Z. F. Ren, and G. Chen, Energy Environ. Sci. **5**, 5147 (2012).
[2] J. Carrete, W. Li, N. Mingo, S. Wang, and S. Curtarolo, Phys. Rev. X **4**, 011019 (2014).
[3] L.-T. Yeh and R. C. Chu, *Thermal Management of Microelectronic Equipment: Heat Transfer Theory, Analysis Methods, and Design Practices* (ASME Press, New York, 2002).
[4] C. D. Wright, L. Wang, P. Shah, M. M. Aziz, E. Varesi, R. Bez, M. Moroni, and F. Cazzaniga, IEEE Trans. Nanotechnol. **10**, 900 (2011).
[5] K. Watari and S. L. Shinde, MRS Bull. **26**, 440 (2001).
[6] G. A. Slack, R. A. Tanzilli, R. O. Pohl, and J. W. Vandersande, J. Phys. Chem. Solids **48**, 641 (1987).
[7] E. S. Toberer, A. Zevalkink, and G. J. Snyder, J. Mater. Chem. **21**, 15843 (2011).
[8] D. A. Broido, M. Malorny, G. Birner, N. Mingo, and D. A. Stewart, Appl. Phys. Lett. **91**, 231922 (2007).
[9] W. Li, N. Mingo, L. Lindsay, D. A. Broido, D. A. Stewart, and N. A. Katcho, Phys. Rev. B **85**, 195436 (2012).
[10] G. Deinzer, G. Birner, and D. Strauch, Phys. Rev. B **67**, 144304 (2003).
[11] A. Ward, D. A. Broido, D. A. Stewart, and G. Deinzer, Phys. Rev. B **80**, 125203 (2009).
[12] A. Ward and D. A. Broido, Phys. Rev. B **81**, 085205 (2010).
[13] Q. Zhang, F. Cao, K. Lukas, W. Liu, K. Esfarjani, C. Opeil, D. Broido, D. Parker, D. J. Singh, G. Chen, and Z. Ren, J. Am. Chem. Soc. **134**, 17731 (2012).
[14] W. Li, L. Lindsay, D. A. Broido, D. A. Stewart, and N. Mingo, Phys. Rev. B **86**, 174307 (2012).
[15] L. Lindsay, D. A. Broido, and T. L. Reinecke, Phys. Rev. Lett. **111**, 025901 (2013).
[16] L. Lindsay, D. A. Broido, and T. L. Reinecke, Phys. Rev. B **87**, 165201 (2013).
[17] J. M. Ziman, *Electrons and Phonons: The Theory of Transport Phenomena in Solids* (Oxford University Press, Oxford, New York, 2001).
[18] J. Callaway, Phys. Rev. **113**, 1046 (1959).
[19] P. B. Allen, Philos. Mag. B **70**, 527 (1994).
[20] M. S. Green, J. Chem. Phys. **22**, 398 (1954).
[21] R. Kubo, J. Phys. Soc. Jpn. **12**, 570 (1957).
[22] S. Curtarolo, G. L. W. Hart, M. Buongiorno Nardelli, N. Mingo, S. Sanvito, and O. Levy, Nat. Mater. **12**, 191 (2013).
[23] M. A. Blanco, E. Francisco, and V. Luaña, Comput. Phys. Commun. **158**, 57 (2004).
[24] S. Curtarolo, W. Setyawan, G. L. W. Hart, M. Jahnatek, R. V. Chepulskii, R. H. Taylor, S. Wang, J. Xue, K. Yang, O. Levy, M. Mehl, H. T. Stokes, D. O. Demchenko, and D. Morgan, Comput. Mater. Sci. **58**, 218 (2012).
[25] S. Curtarolo, W. Setyawan, S. Wang, J. Xue, K. Yang, R. H. Taylor, L. J. Nelson, G. L. W. Hart, S. Sanvito, M. Buongiorno Nardelli, N. Mingo, and O. Levy, Comput. Mater. Sci. **58**, 227 (2012).
[26] R. H. Taylor, F. Rose, C. Toher, O. Levy, K. Yang, M. Buongiorno Nardelli, and S. Curtarolo, Comput. Mater. Sci. **93**, 178 (2014).
[27] A. Jain, G. Hautier, C. J. Moore, S. P. Ong, C. C. Fischer, T. Mueller, K. A. Persson, and G. Ceder, Comput. Mater. Sci. **50**, 2295 (2011).

[28] A. Jain, S. P. Ong, G. Hautier, W. Chen, W. D. Richards, S. Dacek, S. Cholia, D. Gunter, D. Skinner, G. Ceder, and K. A. Persson, APL Mater. **1**, 011002 (2013).
[29] S. P. Ong, W. D. Richards, A. Jain, G. Hautier, M. Kocher, S. Cholia, D. Gunter, V. L. Chevrier, K. A. Persson, and G. Ceder, Comput. Mater. Sci. **68**, 314 (2013).
[30] M. A. Blanco, A. M. Pendás, E. Francisco, J. M. Recio, and R. Franco, J. Mol. Struct.: THEOCHEM **368**, 245 (1996).
[31] J.-P. Poirier, *Introduction to the Physics of the Earth's Interior*, 2nd ed. (Cambridge University Press, Cambridge, 2000).
[32] G. Kresse and J. Hafner, Phys. Rev. B **47**, 558(R) (1993).
[33] P. E. Blöchl, Phys. Rev. B **50**, 17953 (1994).
[34] J. P. Perdew, K. Burke, and M. Ernzerhof, Phys. Rev. Lett. **77**, 3865 (1996).
[35] H. J. Monkhorst and J. D. Pack, Phys. Rev. B **13**, 5188 (1976).
[36] J. C. Slater, *Introduction to Chemical Physics* (McGraw-Hill, New York, 1939).
[37] G. A. Slack, in *Solid State Physics*, edited by H. Ehrenreich, F. Seitz, and D. Turnbull, Vol. 34 (Academic, New York, 1979), p. 1.
[38] D. T. Morelli and G. A. Slack, in *High Thermal Conductivity Materials*, edited by S. L. Shindé and J. S. Goela (Springer, New York, 2006).
[39] D. Wee, B. Kozinsky, B. Pavan, and M. Fornari, J. Electron. Mater. **41**, 977 (2012).
[40] L. Bjerg, B. B. Iversen, and G. K. H. Madsen, Phys. Rev. B **89**, 024304 (2014).
[41] Ioffe Physico-Technical Institute, http://www.ioffe.ru/SVA/NSM/Semicond/index.html
[42] Springer Materials: The Landolt-Börnstein Database, http://www.springermaterials.com/docs/index.html
[43] D. P. Spitzer, J. Phys. Chem. Solids **31**, 19 (1970).
[44] C. R. Whitsett, D. A. Nelson, J. G. Broerman, and E. C. Paxhia, Phys. Rev. B **7**, 4625 (1973).
[45] M. Anis-ur-Rehman and A. Maqsood, Int. J. Thermophys. **24**, 867 (2003).
[46] S. Krukowski, A. Witek, J. Adamczyk, J. Jun, M. Bockowski, I. Grzegory, B. Lucznik, G. Nowak, M. Wróblewski, A. Presz, S. Gierlotka, S. Stelmach, B. Palosz, S. Porowski, and P. Zinn, J. Phys. Chem. Solids **59**, 289 (1998).
[47] G. A. Slack and S. F. Bartram, J. Appl. Phys. **46**, 89 (1975).
[48] C. F. Cline, H. L. Dunegan, and G. W. Henderson, J. Appl. Phys. **38**, 1944 (1967).
[49] G. A. Slack, Phys. Rev. **126**, 427 (1962).
[50] R. H. Bruce and D. S. Cannell, Phys. Rev. B **15**, 4451 (1977).
[51] K. I. Horai, J. Geophys. Res. **76**, 1278 (1971).
[52] J. D. Beasley, Appl. Opt. **33**, 1000 (1994).
[53] J. L. Shay and J. H. Wernick, *Ternary Chalcopyrite Semiconductors: Growth, Electronic Properties, and Applications* (Pergamon, Oxford, New York, 1975).
[54] K. Masumoto, S. Isomura, and W. Goto, J. Phys. Chem. Solids **27**, 1939 (1966).
[55] K. Bohmhammel, P. Deus, and H. A. Schneider, Phys. Stat. Solidi A **65**, 563 (1981).
[56] C. Rincón, M. L. Valeri-Gil, and S. M. Wasim, Phys. Stat. Solidi A **147**, 409 (1995).
[57] K. Bohmhammel, P. Deus, G. Kühn, and W. Möller, Phys. Stat. Solidi A **71**, 505 (1982).
[58] S. C. Abrahams and F. S. L. Hsu, J. Chem. Phys. **63**, 1162 (1975).
[59] P. H. M. Böttger, K. Valset, S. Deledda, and T. G. Finstad, J. Electron. Mater. **39**, 1583 (2010).
[60] P. Türkes, C. Pluntke, and R. Helbig, J. Phys. C: Solid State Phys. **13**, 4941 (1980).
[61] J. Carrete, N. Mingo, S. Wang, and S. Curtarolo, Adv. Funct. Mater. (2014), doi: 10.1002/adfm.201401201.
[62] T. Sekimoto, K. Kurosaki, H. Muta, and S. Yamanaka, Mater. Trans. **46**, 1481 (2005).
[63] Y. Kawaharada, K. Kurosaki, H. Muta, M. Uno, and S. Yamanaka, J. Alloys Compd. **384**, 308 (2004).
[64] Y. Xia, S. Bhattacharya, V. Ponnambalam, A. L. Pope, S. J. Poon, and T. M. Tritt, J. Appl. Phys. **88**, 1952 (2000).
[65] D. P. Young, P. Khalifah, R. J. Cava, and A. P. Ramirez, J. Appl. Phys. **87**, 317 (2000).
[66] H. Hohl, A. P. Ramirez, C. Goldmann, G. Ernst, B. Wölfing, and E. Bucher, J. Phys.: Condens. Matter **11**, 1697 (1999).
[67] C. Uher, J. Yang, S. Hu, D. T. Morelli, and G. P. Meisner, Phys. Rev. B **59**, 8615 (1999).
[68] W. Li and N. Mingo, J. Appl. Phys. **114**, 183505 (2013).